

NUV–IR colours of red sequence galaxies in local clusters

Timothy D. Rawle^{1*}, Russell J. Smith¹, John R. Lucey¹, Michael J. Hudson², Gary A. Wegner³

¹*Department of Physics, Durham University, Durham DH1 3LE, United Kingdom*

²*Department of Physics and Astronomy, University of Waterloo, Waterloo, Ontario, N2L 3G1, Canada*

³*Department of Physics and Astronomy, Dartmouth College, 6127 Wilder Laboratory, Hanover, NH 03755*

14 January 2008

ABSTRACT

We present *GALEX* near-UV (*NUV*) and 2MASS *J* band photometry for red sequence galaxies in local clusters. We define quiescent samples according to a strict emission threshold, removing galaxies with very recent star formation. We analyse the *NUV*–*J* colour–magnitude relation (CMR) and find that the intrinsic scatter is an order of magnitude larger than for the analogous optical CMR (~ 0.35 rather than 0.05 mag), in agreement with previous studies. Comparing the *NUV*–*J* colours with spectroscopically-derived stellar population parameters, we find a strong ($> 5.5\sigma$) correlation with metallicity, only a marginal trend with age, and no correlation with the α/Fe ratio. We explore the origin of the large scatter and conclude that neither aperture effects nor the UV upturn phenomenon contribute significantly. We show that the scatter could be attributed to simple ‘frosting’ by either a young or a low metallicity subpopulation.

Key words: galaxies: elliptical and lenticular, cD – galaxies: stellar content – ultraviolet: galaxies.

1 INTRODUCTION

The optical colour–magnitude relation (CMR) shows that brighter early-type galaxies are also redder (Visvanathan & Sandage 1977), and is traditionally regarded as arising from the mass–metallicity sequence (cf. Dressler 1984, Kodama & Arimoto 1997). Gas loss, caused by supernova wind, occurs earlier in less massive galaxies. Therefore, a smaller fraction of gas is processed before being expelled from the less massive galaxy (Mathews & Baker 1971), resulting in lower average metallicities (Larson 1974). Bower, Lucey & Ellis (1992) found a very small intrinsic scatter in the *U*–*V* CMR (~ 0.05 mag) and, due to the sensitivity of the *U* band to the presence of young stars, interpreted this as a small age dispersion. Age and metallicity are observed to have the same effect on broadband optical colours, whereas spectral line indices can be used to break the degeneracy (Wortheley 1994). Kuntschner & Davies (1998) claimed that the CMR is driven by metallicity variations with luminosity, although Nelan et al. (2005) found evidence for a strong age–mass relation in addition to this metallicity–mass trend (see also Caldwell, Rose & Concannon 2003, Thomas et al. 2005).

The ultraviolet–optical CMR for non-star-forming

galaxies has an intrinsic scatter an order of magnitude larger than its optical counterpart; ~ 0.5 mag compared to 0.05 mag (e.g. Yi et al. 2005). Hot young stellar populations dominate the ultraviolet (UV) flux for ~ 100 Myr after an episode of star formation (ten times longer than $\text{H}\alpha$ emission after star formation; Leitherer et al. 1999). The large intrinsic scatter in the UV CMR is therefore often interpreted as differing quantities of very recent, albeit low level, star formation (Ferreras & Silk 2000).

In intermediate age populations (~ 1 – 3 Gyr), the near-UV (*NUV*; 2000–3000 Å) flux is dominated by hot stars on the main sequence turn-off (e.g. O’Connell 1999). The sensitivity of the turn-off to the epoch of formation emphasises the importance of the UV bands for age determination (Dorman, O’Connell & Rood 2003).

Old (~ 10 Gyr) metal-poor populations have a significant UV flux contribution from very hot ($T_{\text{eff}} \sim 10000\text{K}$) blue horizontal branch (BHB) stars (Maraston & Thomas 2000; Lee, Lee & Gibson 2002). However these tend to reside in globular clusters or galactic haloes (where $\text{Fe}/\text{H} < -1$), where they are useful age indicators (Kaviraj et al. 2007), rather than in relatively metal-rich elliptical galaxies.

The UV picture is further complicated by the presence of the ultraviolet upturn (or UV excess, UVX) phenomenon. First observed by Code (1969), this unanticipated upturn dominates the far-UV (FUV; $< 2000\text{\AA}$)

* E-mail: t.d.rawle@dur.ac.uk

in UVX galaxies. In contrast, the NUV can be decomposed into two separate components: the blue end of the main sequence/subgiant branch, and the UVX contribution (Dorman 1997). Burstein et al. (1988) found that the UVX can sometimes be appreciable at wavelengths as long as 2700Å: for example, in NGC 4649 ~75 per cent of the NUV flux can be attributed to the UVX component. However, the UVX cannot be explained by the BHB population, as the temperature required to fit the upturn would be $T_{\text{eff}} \gtrsim 20000\text{K}$, whereas BHBs are usually no hotter than $T_{\text{eff}} \sim 12000\text{K}$ (O’Connell 1999).

Burstein et al. further reported that FUV flux (assumed to trace the UVX) is strongly correlated with the Mg_2 line strength (\sim metallicity) and also with the velocity dispersion, which is a proxy for galaxy mass. However, more recent studies (e.g. Rich et al. 2005) have weakened the case for a strong UVX vs metallicity relation. From analysis of internal colour gradients, O’Connell et al. (1992) concluded that the FUV flux in most early-types originates from old stellar components. Drawing on these results, the source of the UVX is tentatively identified as hot, low mass, helium burning stars, such as extreme horizontal branch (EHB) or ‘failed’ AGB (AGB-manqué) stars and their progeny (see Yi, Demarque & Oemler 1997, or the review O’Connell 1999).

The *Galaxy Evolution Explorer* (GALEX; launched in 2003; Martin et al. 2005, Morrissey et al. 2007) is revolutionising UV astronomy, with high resolution imaging in two bands: near-ultraviolet (NUV; $\lambda_{\text{eff}} = 2310 \text{ Å}$) and far-ultraviolet (FUV; $\lambda_{\text{eff}} = 1530 \text{ Å}$). Using analysis of both NUV–V and FUV–V vs B–V relations, Donas et al. (2006) suggest that the FUV–NUV colour reflects an extension of the colour–metallicity relation into the UV, as well as deducing that ~10 per cent of ellipticals have residual star formation. Using the NUV–r colour, Kaviraj et al. (2006) also find non-negligible young stellar populations in morphologically selected early-type galaxies. Salim et al. (2007) derive star formation rates (SFRs) from broadband photometry dominated by the UV, and find good agreement with SFRs deduced from spectroscopic indices (predominantly using $\text{H}\alpha$). However, they also confirm that some galaxies with no $\text{H}\alpha$ emission show signs of star formation in the UV bands and attribute this to post-starburst galaxies.

Here, we build upon these previous studies by exploring the relationship between the NUV–J colour and spectroscopic stellar population indicators for a sample of quiescent, red sequence galaxies in nearby clusters. This paper is organised as follows. Section 2 describes our two red sequence samples and associated 2MASS and GALEX datasets. The criteria used to remove galaxies with emission are described. In Section 3 we show that a large intrinsic scatter is found in the NUV–J colours of these quiescent cluster galaxies. Metallicity is shown to be strongly correlated with the NUV–J colour, although there remains a large residual scatter. Section 4 discusses possible explanations for this scatter, showing that morphological abnormalities, aperture bias and the UV upturn do not contribute significantly. We investigate simple ‘frosting’ models with a low mass fraction of younger stars (or alternatively a low mass fraction population of low metallicity, blue horizontal branch stars), and show that these could account for the scatter. The uncertainties in the

NUV K-correction are also discussed. Our conclusions are given in Section 5.

2 DATA

We use two complementary samples of red sequence galaxies in local clusters: the first is explicitly red sequence selected by optical colour, and is a large sample, containing ~10 times the number of galaxies; the second has the advantage of higher quality spectroscopy, and uses an emission line cut (Sec. 2.3) to ensure a red sequence sample. Smith et al. (2007) Fig. 1 demonstrates that $\text{H}\alpha$ selection efficiently removes all galaxies bluer than the red sequence and is more restrictive than a cut on colour.

2.1 Galaxy samples

2.1.1 NFPS sample

The NOAO Fundamental Plane Survey (NFPS; Smith et al. 2004, Nelan et al. 2005) is a study of X-ray selected clusters distributed over the whole sky and at redshifts between $0.015 < z < 0.072$. More than 4500 galaxies lying within 1 Mpc of the centre of each cluster, and within 0.2 mag of the cluster red sequence on the B–R CMR (see Smith et al. 2004 Fig. 3), were observed spectroscopically. Of these, 3514 have redshift, velocity dispersion and spectral line strength measurements (from 2 arcsec diameter fibres).

2.1.2 Shapley Supercluster (SSC) sample

The second sample of galaxies concentrates on the core of the Shapley supercluster (SSC; Abell clusters A3556, A3558, A3562 at $z \approx 0.049$). This sample consists of 541 galaxies selected from NFPS imaging but to a deeper limit ($R < 18$; Smith et al. 2007). Follow-up spectroscopy for these targets were obtained using 2 arcsec diameter fibres, equating to 2 kpc at the distance of Shapley. A set of three non-redundant line indices were fit to the models of Thomas et al. (2003, 2004) in order to estimate age, metallicity (Z/H) and α -abundance (α/Fe) for each galaxy. The primary tracer of age in this scheme is $\text{H}\gamma\text{F}$; for metallicity Fe5015 is used; $\text{Mgb}5177$ is the α -abundance indicator. This method is described in detail in Smith et al. (in prep.).

2.2 GALEX and 2MASS data

Galaxy Evolution Explorer (GALEX) near-ultraviolet (NUV) band images are available for 26 (from a total of 93) NFPS clusters. Due to a detector fault, only some clusters have associated far-ultraviolet (FUV) band images. Most of the images are from our guest investigator snapshot programme (GALEX GI1_004) which targeted a subset of NFPS clusters with low galactic extinction and having a large number of spectra from Smith et al. (2004). In addition, a small number of images of comparable depth from the GR2 GI archive, medium imaging survey (MIS) and near galaxy survey (NGS) have been used. Table 1 lists all the images analysed along with their centre position and stacked exposure time. GALEX images have a 1.25° diameter, but only the central 1.2° field has been analysed due to the poor image

Table 1. GALEX *NUV* images. cz (km s⁻¹) is cluster redshift in the CMB frame. A single exposure is used unless column six indicates the number of coadded images. Total exposure time for coadded images is given for *NUV* and (where the image is available) *FUV*.

GALEX image	Centre RA (J2000)	Centre Dec (J2000)	Cluster(s)	cz_{CMB} (km s ⁻¹)	Images coadded	t_{exp} (secs)	
						<i>NUV</i>	<i>FUV</i>
GI1_004001_A2734	00 11 21.6	-28 51 00	A2734	18249	3	3535	
GI1_067001_UGC0568_0003	00 55 08.9	-01 02 47	A0119	12958		1556	3024
MISDR1_16976_0422	01 14 29.3	+15 01 46	A0160A	12794		1444	1444
GI1_004002_A0262_0001	01 52 45.6	+36 08 58	A0262	4464		1698	1698
NGA_NGC1058	02 43 26.6	+36 25 39	A0376	14371		1265	1265
GI1_004003_A3104_0001	03 14 21.6	-45 25 12	A3104	21560		1588	1588
GI1_004027_A3158_0001	03 42 57.6	-53 37 48	A3158	17542		1026	887
GI1_004004_A3266	04 31 24.0	-61 26 24	A3266	17713	2	1441	1441
GI1_004005_A0548	05 46 40.0	-25 37 21	A0548A/B	12439	4	3155	
GI1_004006_A3376	06 01 43.2	-39 59 24	A3376	14016	2	2176	2176
GI1_004007_A3389_0002	06 21 57.7	-64 57 35	A3389	8075		976	
MISDR1_24335_0270	10 13 07.7	-00 23 25	A0957	13849		1703	1703
GI1_004025_A3528_0001	12 53 57.6	-29 13 48	A3528A/B	16764		1697	
GI1_004008_A1644_0002	12 57 12.0	-17 24 36	A1644	14478		1163	
GI1_009003_HP J1321m31_0001	13 21 05.8	-31 32 20	A3556	14660		1615	
GI1_004010_A3556	13 25 26.1	-31 36 07	A3556, A3558	14660	2	1805	
GI1_004011_A3558_0001	13 27 57.6	-31 30 00	A3558	14660		1676	
MISDR1_33707_0586	14 42 46.3	+03 39 11	MKW8	8449		1698	1698
GI1_004016_A1991_0001	14 54 31.1	+18 38 23	A1991	17741		967	
GI1_004026_A2063_0001	15 23 36.0	+08 36 34	A2063	10444		1512	
NGA_NGC6166	16 28 39.9	+39 33 24	A2199	8872		1437	1437
GI1_004020_A3716	20 51 57.5	-52 46 48	A3716	13141	2	3179	1689
GI1_004021_A2399_0004	21 57 19.1	-07 47 59	A2399	17046		1322	
GI1_004022_A2589	23 23 57.6	+16 46 47	A2589	12001	3	4252	
GI1_004023_A4059_0003	23 56 59.9	-34 45 35	A4059	14660		635	

quality at the edges. *GALEX* images have a plate scale of 1.5 arcsec pixel⁻¹ and a PSF FWHM of ~ 5 arcsec.

We analyse infrared tiles from the *J* band ($\lambda_{\text{eff}} = 1.25\mu\text{m}$) of the Two Micron All Sky Survey (2MASS; Skrutskie et al. 2006). We measure directly from the tiles, rather than adopt photometry from the 2MASS extended source catalogue (XSC; Jarrett et al. 2000), as some of our target objects are unresolved. Additionally, we require the PSF to match that of the *NUV* images (2MASS *J* PSF FWHM ~ 3 arcsec) and therefore Gaussian smooth the 2MASS tiles before analysis. 2MASS tiles have a plate scale of 1 arcsec pixel⁻¹.

SEXTRACTOR (Bertin & Arnouts 1996) was employed in dual image mode to detect all objects in the *J* band. Photometry was measured for all sample targets in both bands using a range of matched apertures: a Kron-type aperture (SEXTRACTOR's MAG_AUTO) and seven apertures 3–34.5 arcsec in diameter (MAG_APER). Throughout this work, *J* band Kron apertures are used for total luminosity, and matched 12 arcsec diameter apertures for *NUV*–*J* colours. Our *J* band photometry is in good agreement with 2MASS (~ 0.2 mag RMS) for objects in the XSC.

Targets with SEXTRACTOR apertures flagged as truncated, or with a deblending error, have been removed from the sample, and only confirmed cluster members with redshift and $\log \sigma$ measurements within the Smith et al. (2004) or Smith et al. (2007) datasets (NFPS and SSC respectively) are used in the analysis. Table 2 lists the number of galaxies in the samples at this stage, and after subsequent restrictions.

All colours and magnitudes are measured in the

Table 2. Size of the galaxy samples, following the selection criteria applied.

	NFPS	SSC
Original sample	4527	541
...with usable <i>NUV</i> and <i>J</i> photometry	1493	307
...with cz and $\log \sigma$ data	990	267
...after emission line cut	920	156
.....after optical apparent magnitude cut ¹	544	101
.....with stellar population parameters ²	–	87
.....with <i>FUV</i> and H γ F data ³	222	–

NOTE – see ¹(Sec 3.1), ²(Sec 3.2) or ³(Sec 4.2)

AB system ($J_{\text{AB}} = J_{\text{Vega}} + 0.91$; Blanton et al. 2005), and have been corrected for galactic extinction using the reddening maps of Schlegel, Finkbeiner & Davies (1998); $A_{\text{FUV}} = 8.29 \times E(B-V)$, $A_{\text{NUV}} = 8.87 \times E(B-V)$, $A_J = 0.902 \times E(B-V)$ (Cardelli, Clayton & Mathis 1989; Schlegel et al.).

Estimates of the K-correction in the UV bands are currently derived empirically from poorly constrained spectra, and therefore subject to large uncertainties. Kaviraj et al. (2006, fig. 22) estimate that the *NUV*–*i* correction would be ~ 0.1 mag throughout the range in redshift considered here. We do not apply a K-correction in this study. This issue is addressed further in Section 4.4.

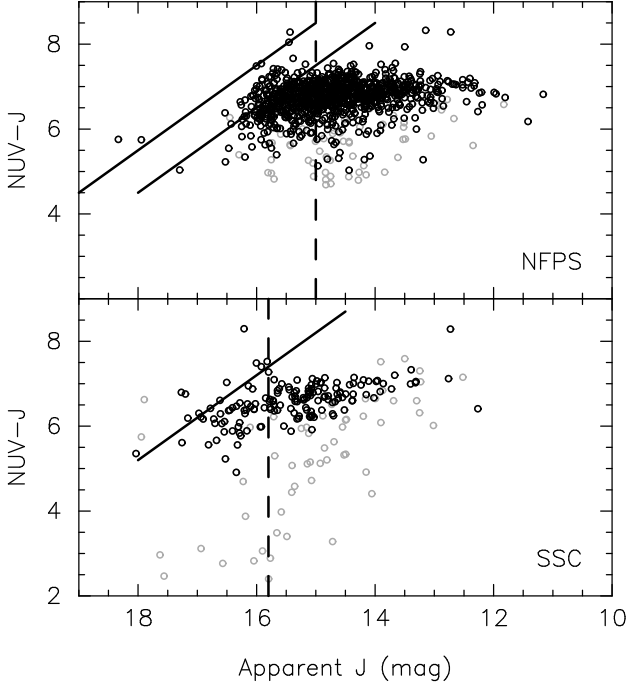


Figure 1. Colour-magnitude diagram for the samples (NFPS upper panel; SSC lower panel). Grey points are those removed by emission line criteria detailed in Sec. 2.3. The larger tail of grey points for SSC results from the lack of an explicit colour cut on the original sample. Solid lines are *GALEX* detection limits and dashed lines are the applied *J* band apparent magnitude cuts. Median error bars are ~ 0.05 mag in *J* band and ~ 0.1 mag in the colour.

2.3 Emission-line cuts

In order to construct a sample of emission-free red sequence galaxies, a restriction is made on emission line strengths. Mindful of the effect of nebular emission ‘fill in’ for the age-sensitive Balmer lines ($H\beta$, $H\gamma$ and $H\delta$), the preferred cut is on the $H\alpha$ line. Unfortunately, $H\alpha$ was not measured for most NFPS galaxies, so the selection criteria of the original NFPS reduction has been adopted (Nelan et al. 2005). Specifically, this involves a cut on the $H\beta$ equivalent width, $EW(H\beta) > -0.6$ Å (negative EW denotes spectral line emission) supplemented by a cut on OIII $\lambda 5007$, $EW(\text{OIII } \lambda 5007) > -0.8$ Å. The cut on the SSC sample, which has $H\alpha$ measurements, follows the prescription of Smith et al. (2007), which uses $EW(H\alpha) > -0.5$ Å (approximately equivalent to $EW(H\beta) > -0.2$ Å). The OIII cut would not remove any additional galaxies. These cuts ensure red sequence subsamples, free of galaxies with a sizeable star formation component or an optically strong active galactic nucleus. The data and photometry for the resulting subsamples are reported in Tables 3 and 4.

3 RESULTS

3.1 *NUV-J* colour relations

Figure 1 shows the *NUV-J* colour-(apparent) magnitude diagram for the NFPS and SSC samples. Shown in grey are

the galaxies removed by the emission cut from Section 2.3. Prior to the emission cut, SSC has a larger colour range than NFPS. This is because NFPS was explicitly selected on *B-R* colour while SSC only on total *R* band apparent magnitude. The $H\alpha$ cut efficiently removes the very blue objects.

All target galaxies were within the 2MASS *J* band detection limit, but the *NUV* band has a 5σ detection limit of 22.5–23.5 mag, depending on the coadded image exposure time. Figure 1 (upper panel) shows that for the NFPS, these limits result in a bias against faint red galaxies. Assuming the brightest *NUV* detection limit, a sample cut is applied to the *J* band apparent magnitude at 15.0 mag. For the SSC sample, all of the targets appear on just two *NUV* images with similar exposure times, and a (5σ) detection limit of 23.2 mag. Although in practice only two SSC targets have a non-positive flux in the *NUV* band (compared to ~ 8 per cent in NFPS), for consistency, SSC has been treated in a similar manner, with a cut applied at 15.8 mag. These cuts are shown as dashed lines in Figure 1 and ensure a complete sampling of the colour range over the selected luminosity interval.

The colour-(absolute) magnitude diagrams for the low-emission galaxies are presented in Figure 2. There is a correlation between the luminosity and colour; brighter galaxies tend to be redder. However, there is a large scatter; rms dispersions of 0.37 and 0.30 mag for NFPS and SSC samples respectively. The smaller scatter within the SSC sample is probably due to the slightly more restrictive Balmer emission line criteria (see Sec. 2.3). The scatter in each sample does not increase by more than ~ 10 per cent unless the cut criteria are relaxed beyond an equivalent width of -1 Å. Only 5 per cent of the scatter can be accounted for by photometric measurement error. As intrinsic scatter dominates, all correlations in this study are computed without error weighting.

Table 5 summarises the CMRs for our two samples. Additionally, the CMRs measured in three previous studies (Yi et al. 2005, Boselli et al. 2005, Haines, Gargiulo & Merluzzi 2007) are shown for comparison. Different sample selections were used for each of these studies. Yi et al. use a ‘UV-weak’ early-type galaxy sample, selected from SDSS by concentration index and luminosity profiles, and then by the flux ratios $F(\text{NUV})/F(r)$ and $F(\text{FUV})/F(r)$ both being less than 0.07. The sample covers a *J* band luminosity range comparable to our work. Boselli et al. use a volume-limited sample of galaxies in the Virgo cluster, with a subsample defined as elliptical by visual classification. Haines et al. use a volume limited sample of local galaxies from SDSS, with the subsample (labelled ‘passive red sequence galaxies’) restricted by the emission line criteria $EW(H\alpha) > -2$ Å.

Despite these selection differences, our derived relations are in good agreement with the previous studies. The scatter is consistent (~ 0.3 – 0.5 mag) given the different sample definitions, and considerably large in comparison to that of the optical CMR (~ 0.05 mag; Bower et al. 1992).

Velocity dispersion provides an alternative mass proxy to luminosity, and, for optical colours, the σ correlation appears more fundamental (Bernardi et al. 2005). Figure 3 presents the samples in terms of their *NUV-J* colour and $\log \sigma$. There is a clear correlation, with slopes of 0.73 ± 0.11 and 0.65 ± 0.17 for NFPS and SSC respectively, but the rms

Table 3. Data for galaxies in the NFPs sample. Galaxy position is encoded in the ID. cz_{CMB} (km s^{-1}) is the mean cluster redshift in the CMB frame. cz_{hel} (km s^{-1}) is galaxy redshift in the heliocentric frame. Magnitudes (Kron-type apertures) and colours (12 arcsec diameter apertures) are in the AB system and have been galactic extinction corrected, but not K-corrected.

Galaxy ID	cluster cz_{CMB}	galaxy cz_{hel}	apparent J	$NUV-J$	$FUV-J$
NFPJ043305.0-612235	17714	16144	15.750 ± 0.071	6.732 ± 0.142	7.205 ± 0.250
NFPJ043306.7-612614	17714	17702	14.898 ± 0.047	7.091 ± 0.102	7.497 ± 0.184
NFPJ043307.6-611338	17714	16356	14.659 ± 0.042	6.979 ± 0.095	7.659 ± 0.195
NFPJ054415.7-255429	12939	10674	14.693 ± 0.045	6.886 ± 0.077	-
NFPJ054431.6-255550	12939	13247	14.783 ± 0.047	6.767 ± 0.086	-

Full content of this table is available in the electronic version

Table 4. Data for galaxies in the SSC sample. As in Table 3. Supercluster mean $cz_{\text{CMB}} = 14660 \text{ km s}^{-1}$ for all galaxies. Stellar population parameters given where available (age in Gyr).

Galaxy ID	cz_{hel}	apparent J	$NUV-J$	$\log(\text{age/Gyr})$	$[Z/H]$	$[\alpha/\text{Fe}]$
NFPJ132418.2-314229	13948	14.197 ± 0.035	7.088 ± 0.085	0.94 ± 0.03	0.27 ± 0.02	0.24 ± 0.02
NFPJ132423.0-313631	14642	14.847 ± 0.048	6.706 ± 0.103	0.89 ± 0.05	0.11 ± 0.03	0.15 ± 0.02
NFPJ132425.9-314117	13888	14.380 ± 0.038	6.604 ± 0.079	-	-	-
NFPJ132426.5-315153	14922	14.676 ± 0.043	6.575 ± 0.081	0.95 ± 0.04	0.23 ± 0.03	0.24 ± 0.02
2MASXJ13250387-3132449	14266	14.792 ± 0.049	6.626 ± 0.109	-	-	-

Full content of this table is available in the electronic version

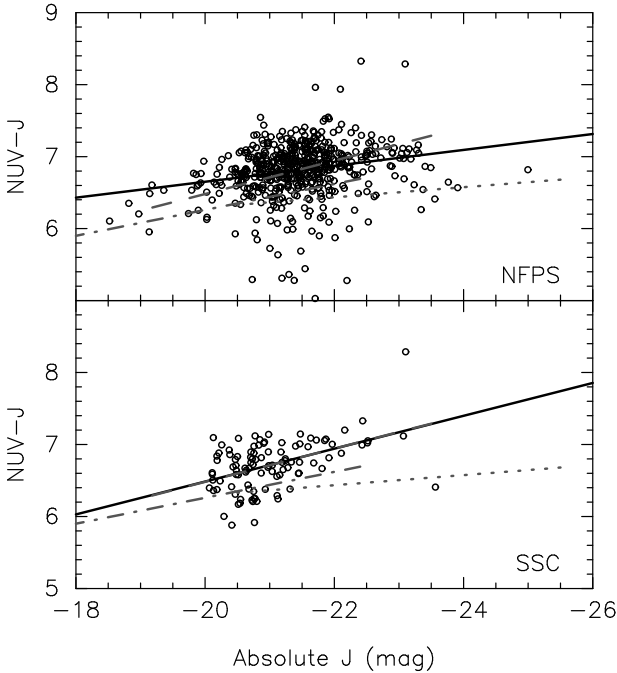


Figure 2. $NUV-J$ colour-absolute magnitude diagram for both samples, with best fits in black. Relations from previous studies in grey: Yi et al. (2005)=dashed, Boselli et al. (2005)=dotted, Haines, Gargiulo & Merluzzi (2007)=dash-dotted. Median error bars are ~ 0.05 mag in J band and ~ 0.1 mag in $NUV-J$.

scatter (0.36 and 0.32 mags) is indistinguishable from that of the CMR.

Figure 4 shows the fraction of ‘blue’ galaxies as a function of $\log \sigma$ for our two samples. Blue galaxies are defined by $NUV-J < 6.4$ mag, as used in Schawinski et al. (2006) who study SDSS galaxies probing to much lower density en-

Table 5. $NUV-J$ CMRs.

	original x	original y	transformed a	transformed b	rms dispersion
NFPs	J	$NUV-J$	-0.11	4.45	0.37
SSC	J	$NUV-J$	-0.23	1.93	0.30
Y05 ¹	r	$NUV-r$	-0.23	1.88	0.58
B05 ²	H	$NUV-H$	-0.07	4.89	0.47
H07 ³	r	$NUV-r$	-0.18	2.66	0.37

NOTES – Original x and y parameters are given for reference. a and b are for relations in the form $NUV-J = aJ + b$, assuming the following colours: $(J-H)_{\text{AB}}=0.2$, $R_{\text{AB}}=r-0.21$, $(J-R)_{\text{AB}}=-0.8$. ¹from Yi et al. (2005). ²from Boselli et al. (2005). ³from Haines, Gargiulo & Merluzzi (2007).

vironments than our samples. Their blue galaxy fractions are plotted in Fig. 4 and show a markedly higher fraction for a given velocity dispersion. For example, our two samples have a blue fraction of ~ 40 per cent only at the lowest sigma ($\log \sigma < 1.8$), while the Schawinski et al. sample reaches this blue fraction at $\log \sigma = 2.2$. At face value, this result suggests a large difference between field and cluster galaxy populations. However, the differences in sample selection have to be considered (Schawinski et al. use a sample selected on morphology), which is beyond the scope of this study.

3.2 Stellar population parameters in the Shapley sample

In order to investigate the physical origin of the large intrinsic scatter found in the $NUV-J$ colour, we examine the relationship between colour and the stellar population pa-

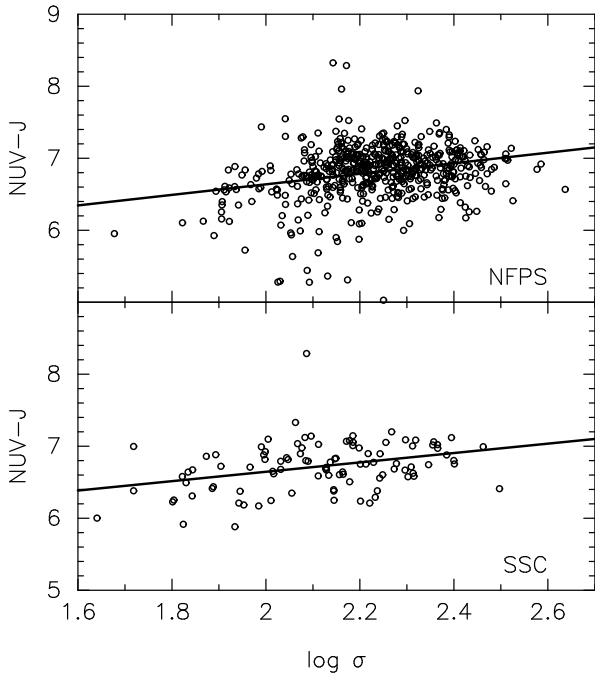


Figure 3. $NUV-J$ vs $\log \sigma$ for NFPS (upper panel) and SSC (lower panel). Median error bars are ~ 0.02 and ~ 0.01 for $\log \sigma$ in the two samples respectively and ~ 0.1 in the colour.

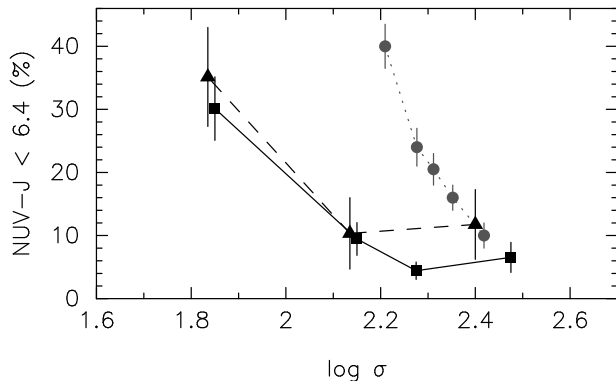


Figure 4. Fraction of galaxies with $NUV-J < 6.4$ as a function of $\log \sigma$. NFPS: squares/solid line; SSC: triangles/dashed line. Estimates from Figure 1 of Schawinski et al. (2006) are given for comparison (circles/dotted line) and show a much steeper increase in the number of blue galaxies with decreasing σ .

rameters (age, metallicity, α -abundance) for the SSC sample.

In the following analysis, involving only the SSC sample, the derived limit on J band apparent magnitude (Sec. 3.1) is not applied, allowing a larger number of galaxies. (It should be noted that the subsequent conclusions are robust against the use of the J band cut.) The emission line selection criteria *are* retained, and the sample is further restricted by the overlap of the photometric and spectroscopic datasets (see Table 2).

$NUV-J$ vs $\log(\text{age})$ is shown in Figure 5 (upper panel). Galaxies with nebular emission have been removed via the emission line criteria. Therefore, if the UV sources also contribute to the optical flux and have strong Balmer lines, the

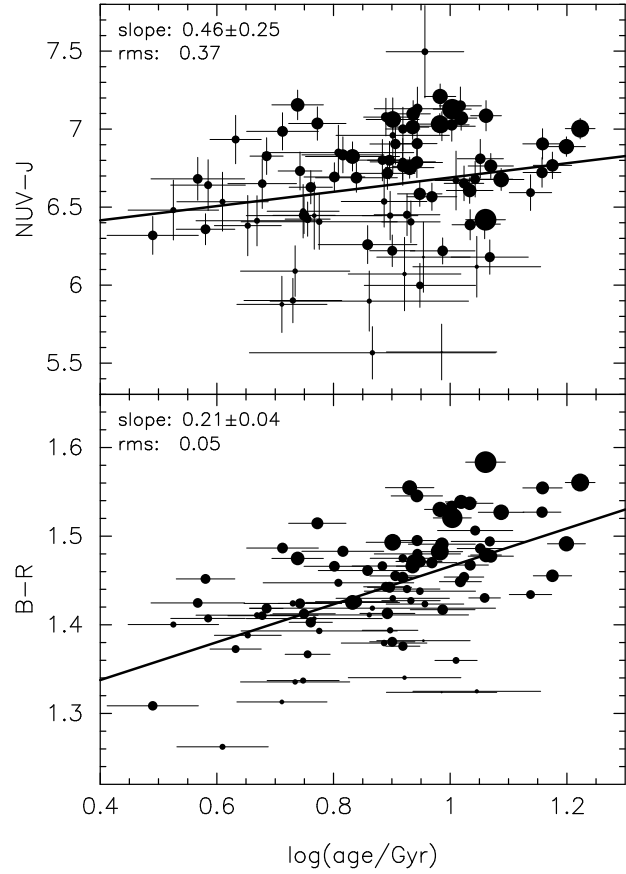


Figure 5. $NUV-J$ (upper) and $B-R$ (lower; from Mercurio et al.) colours vs $\log(\text{age})$ for the SSC sample. Symbol size represents J band luminosity; larger=brighter. Note that the lower panel has a much smaller range in the vertical scale.

$NUV-J$ and age for the remaining objects would be correlated. We find only a marginal correlation between age and $NUV-J$, with a slope of 0.46 ± 0.25 and an intrinsic scatter (after accounting for the measurement error) of 0.33 mag. From the upper panel of Fig. 5, it is also apparent that more luminous, and by inference larger, red sequence galaxies (J band luminosity is shown in Figs. 5–7 by the symbol size) are not solely confined to the redder $NUV-J$ colours, although they do tend to be the oldest.

Figure 5 (lower panel) shows the relation between age and $B-R$ colour for the same sample of galaxies (note the much smaller range in the vertical scale). There is a strong correlation; a slope of 0.21 ± 0.04 and rms dispersion of 0.05 mag. This figure confirms that the NUV scatter is not due to contamination by optically blue galaxies.

The analogous $NUV-J$ correlation with the metallicity is given in Figure 6. There is a strong trend between $[Z/H]$ and $NUV-J$, with a slope of 1.27 ± 0.23 and an rms dispersion of 0.32 mag (~ 90 per cent of which is intrinsic scatter). The lack of galaxies to the top left is not the result of a selection effect. Of the two target galaxies undetected in the NUV band (see Sec. 3.1), only one has a low metallicity. Assuming the non-detection is due to a redder-than-average colour, this would add a single galaxy to the upper left of the plot, but would not significantly

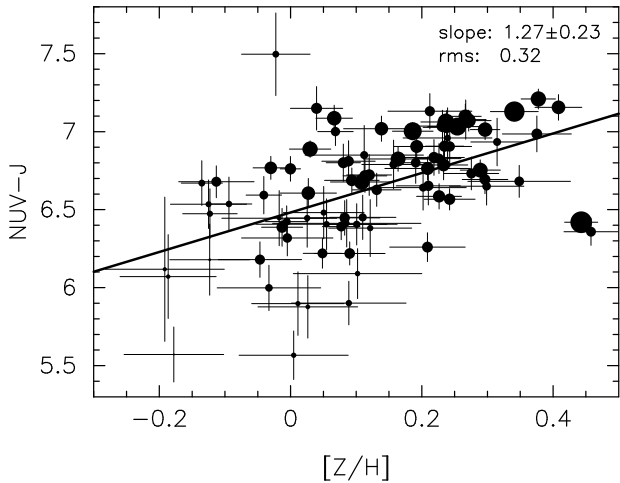


Figure 6. $NUV-J$ vs metallicity $[Z/H]$. Symbol size represents J band luminosity; larger=brighter.

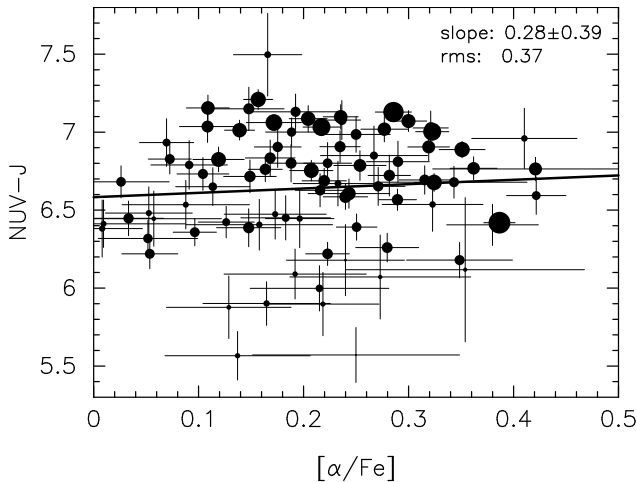


Figure 7. $NUV-J$ vs α -abundance $[\alpha/Fe]$. Symbol size represents J band luminosity; larger=brighter.

affect the fit. In general, the most luminous galaxies form a ridgeline at redder colours, although there are significant bright outliers to this trend (the most obvious being the bright, blue, metal-rich galaxy on the right; NFPJ132729.7–312325). Lower metallicity galaxies tend to be bluer and less luminous. This supports Rampazzo et al. (2007), who use simulations to predict a correlation of $NUV-IR$ colour with metallicity, but little dependence on age in populations greater than 2–3 Gyr after a star formation episode. However, the slope of our observed metallicity trend is 2–3 times weaker than that derived from theoretical spectra by Dorman, O’Connell & Rood (2003).

Model evolutionary tracks suggest that stellar evolution depends on α/Fe (Salasnich et al. 2000; Dotter et al. 2007). However, we find no discernible relation between the $NUV-J$ colour and the α -abundance in this sample of red sequence galaxies (rms scatter of 0.37 mag; Fig. 7).

Figure 8 shows the residuals from the NUV vs metallicity relation (Fig. 6) against $\log(\text{age})$. Although the residuals are more strongly correlated with age ($\sim 3\sigma$) than the colours themselves are, the rms dispersion is only reduced to

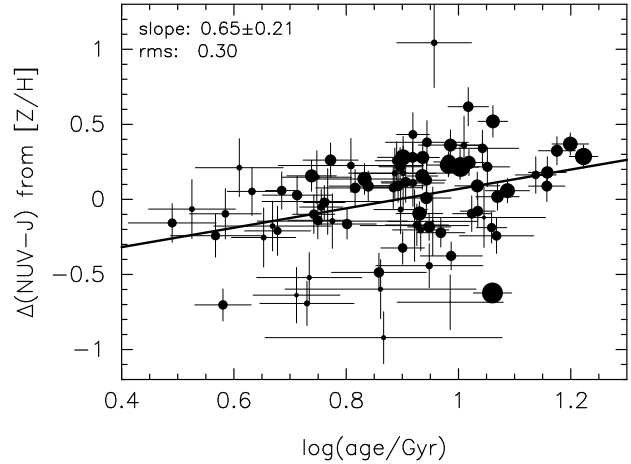


Figure 8. $NUV-J$ residuals from the $[Z/H]$ relation vs $\log(\text{age})$. Symbol size represents J band luminosity; larger=brighter.

0.3 mag (~ 0.25 mag intrinsic scatter). This is in contrast to the case of the $B-R$ colour where the majority of the scatter can be attributed to age and metallicity (Smith et al. in prep.).

4 DISCUSSION

This section explores possible causes of the large intrinsic scatter observed in the $NUV-J$ colour. We investigate aperture bias, the UV upturn phenomenon and ‘frosting’ by young or metal poor subpopulations. Additionally, we comment on the uncertainty in the NUV band K-corrections.

4.1 Aperture bias/morphology

The spectroscopy used to estimate the stellar parameters is derived from 2 arcsec diameter fibres, whilst the $NUV-J$ colours are from 12 arcsec diameter aperture photometry. Eliminating aperture bias completely would require matched apertures for the photometry and spectroscopy, but unfortunately the PSF of the 2MASS and *GALEX* images is too large for reliable 2 arcsec aperture photometry.

Broadband colours and spectroscopic measurements (e.g. Tamura & Ohta 2004, Sánchez-Blázquez et al. 2007) show that elliptical galaxies generally have flat radial profiles in age, and regular metallicity gradients (decreasing $[Z/H]$ with radius). The aperture effect therefore flattens the $NUV-J$ vs Z/H relation, as larger, redder galaxies will tend to exhibit higher metallicities within the fibre. However, the effect is small, with only ~ 0.1 dex change in metallicity over a 1 dex difference in aperture radius.

Inspection of the galaxies in high resolution images can ascertain whether there are morphological peculiarities, or neighbouring objects, contributing to an enhanced large radius NUV flux. Figure 9 shows colour vs age and metallicity (as in Figs. 5–6), highlighting the few galaxies that have high resolution *HST*-ACS images available. Fortunately, one of these objects is the most obvious outlier in the whole sample (NFPJ132729.7–312325); it is the reddest in $B-R$, but has an unusually blue $NUV-J$ colour for such a metal-rich, luminous galaxy. In the *HST*-ACS image (Fig. 10), the

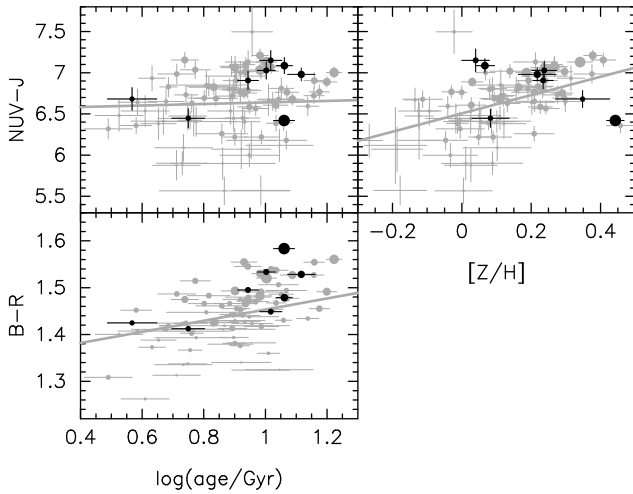


Figure 9. Colour vs stellar parameters, highlighting galaxies with available *HST*-ACS images. Symbol size reflects *J* band luminosity (larger=brighter). In all cases, ACS confirms early-type morphology, uncontaminated by neighbours.

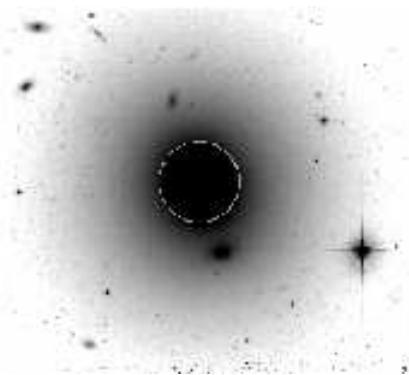


Figure 10. *HST*-ACS image of the outlier NFPJ132729.7-312325, with a 12 arcsec diameter aperture marked.

galaxy appears to be a large elliptical with no abnormalities. There are also no obvious contaminating objects that could be responsible for an anomalous blue colour.

On close examination, the other targets with *HST*-ACS images also appear to be ‘normal’ ellipticals of various sizes, with no obvious peculiarities or large radius *NUV* contributors. We conclude that a large scatter in *NUV*–*J* colour is present even in objects with confirmed regular early-type morphologies and no contaminants. Additionally, a scatter of ~ 0.3 – 0.35 mag is still obtained when smaller matched apertures (4.5 arcsec diameter) are used for the colour, despite the probability of a contaminating neighbour being reduced by ~ 85 per cent.

4.2 UV upturn

Another possible explanation for the scatter in *NUV*–*J* colour is *NUV* contamination by the UV upturn (UVX). The Thomas et al. (2003) models used in the stellar populations parameter calculations include low-metallicity blue horizontal branch sub-populations and thermal pulsing asymptotic giant branch stars, but they do not include the

low mass, metal-rich, helium burning stars with small envelopes currently thought to be the most likely candidate for the UV upturn (O’Connell 1999). The UV upturn is one of the most heterogeneous photometric properties of old stellar populations in early-type galaxies, with a spread of up to ~ 4 magnitudes in the *FUV* (O’Connell 1999), so certainly seems a plausible explanation for the scatter.

The hot UVX component appears in the spectra as a smooth continuum with an absence of emission and absorption lines. Hence, the *FUV* flux from a galaxy can be used to estimate the extent of the contribution in the *NUV* band (Burstein et al. 1988). Unfortunately, none of the SSC galaxies have available *FUV* photometry, so in order to estimate the extent of the UVX contribution, the corrections are calculated for all objects in the NFPS sample that have the necessary *FUV* data. However, stellar population ages have not been derived for individual NFPS galaxies, so instead we compare the corrected *NUV*–*J* colours to the traditional ‘age-tracing’ Balmer line $H\gamma F$. This line does not trace age cleanly, being affected to a small degree by the metallicity.

$H\gamma F$ vs *NUV*–*J* for the NFPS sample is shown in Figure 11. Given the relative strengths of the colour vs. age and $[Z/H]$ relations (Figures 5 and 6), the correlation seen here is most likely a reflection of the metallicity, rather than age, dependence of $H\gamma F$. For comparison, the observations have been overlaid by age/metallicity grids constructed from the models of Maraston (2005, M05; upper panel) and Bruzual & Charlot (2003, BC03; lower panel). Both grids lie redward of the observed data, most likely due to neither model including EHB stars, although the BC03 grid provides the better description of the data. Previous studies (e.g. Salim et al. 2007) have noted that while the BC03 models do not explicitly include EHB stars, the UV light from old stellar populations (primarily post-AGB stars) reproduce several of the correlations found in observational data, including the relation between *FUV*–*NUV* and *B*–*V* colours (see Donas et al. 2006, particularly fig. 5).

Dorman, O’Connell & Rood (2003) introduced corrections to their *NUV*–*V* colours by considering the relative contributions of the hot and cool (i.e. non-UVX) components at *FUV*, *NUV* and *V*. They assumed a negligible contribution of the cool component to the *FUV* flux, but allowed hot stars to contribute at *V*. Here, we use analogous corrections for the *NUV*–*J* colours, which are simpler because it is safe to assume no UVX contribution at *J*. The corrected colours are given by

$$(NUV - J)_{\text{corr}} = -2.5 \times \log[10^{-0.4(NUV-J)_{\text{obs}}} - \alpha \times 10^{-0.4(FUV-J)_{\text{obs}}}] \quad (1)$$

where $\alpha \approx 0.3$ is the ratio of *NUV* to *FUV* flux for the hot component (appropriate for a $T_{\text{eff}} = 24000$ K star, see Dorman et al.).

The resulting corrections are shown as vertical lines in Figure 12 (where the points indicate the value of the corrected colour). The corrections move the colours redward as expected, but are only of the order of ~ 0.2 magnitudes, and do not reduce the scatter in the *NUV*–*J* (0.29 mag before corrections, 0.30 mag after). Obviously there are no extreme UVX galaxies with large hot component contributions to the *NUV* flux in this sample, and as such the UVX phenomenon is unlikely to responsible for the scatter in *NUV*–

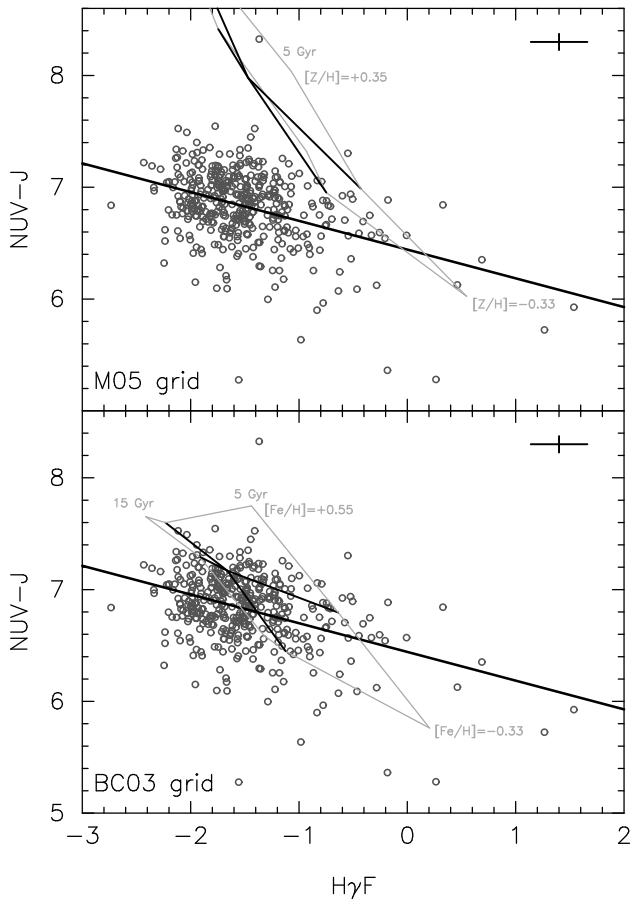


Figure 11. $NUV-J$ (without K-correction) against $H\gamma F$ Balmer index for NFPS galaxies. Upper panel: M05 grid (age={5,12,15 Gyr}, $[Z/H]=\{-0.33,0.00,+0.35\}$). Lower panel: BC03 grid (age={5,12,15 Gyr}, $[Fe/H]=\{-0.33,+0.09,+0.55\}$). (5,-0.33) is the bluest (age, $[Z/H]$) grid point. Median error bars are shown top right.

J for NFPS. We speculate that the UVX effects in the SSC sample are smaller because, on average, the galaxies have lower luminosities.

4.3 Stellar population ‘frosting’

The simple models can be generalised by constructing composite stellar populations. A common invocation of this is residual star formation in the form of ‘frosting’ galaxies with a small mass fraction of young stars (Trager et al. 2000), which manifests itself in the observables as a bluer colour and a younger age than the base population. Frosting should not affect the spectroscopic metallicity or α -abundance significantly as these are primarily driven by the larger, older population (Serra & Trager 2007).

Figure 13 shows the extent to which frosting can account for the scatter, after the effect of metallicity has been removed using the correlation of Fig. 6. Simple stellar population (SSP) tracks from both the M05 and BC03 models are shown. The slope of the BC03 track fits the observed red envelope well, whereas M05 predicts a much steeper variation with age. Allowing for the systematic effects of aperture bias and the UV upturn (~ 0.3 mag bluer in observed $NUV-J$),

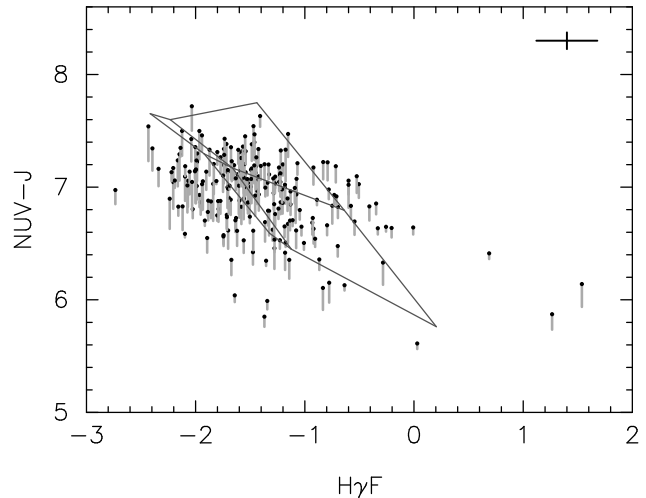


Figure 12. $NUV-J$ (without K-correction) against $H\gamma F$ Balmer index for galaxies with available FUV data. Points indicate the corrected colour, with the ‘tail’ showing the correction vector. BC03 grid as in Fig. 11 (lower panel). Median error bars are shown top right.

~ 30 per cent of the galaxies cannot be accounted for by the SSP model.

Vectors of the frosting effect on $NUV-J$ colour and spectroscopic age have been calculated using the BC03 models. Frosting of a 15 Gyr base population by a 1.5 Gyr population with a mass fraction $\mu=0.03$, and by a 0.7 Gyr population of $\mu=0.01$ are shown. The M05 models result in marginally steeper frosting vectors, as would be expected given the steeper SSP track. The vectors show that frosting, even at a modest level of 1–2 per cent for a ~ 1 Gyr population, could account for a sizeable portion of the scatter in the $NUV-J$ colour. A young population of this size would not be apparent in the $B-R$ colours.

The spectroscopic age is sensitive to frosting via the increased hot-star contribution to the Balmer lines, and for a given change to the spectroscopic age, the UV colours are affected more strongly by frosting than by lowering the age of a single-burst population. This supports the assertion that UV colours are partly dependent on low level recent star formation (Ferrerias & Silk 2000, Kaviraj et al. 2006, Salim et al. 2007). However, there are spectroscopically old galaxies with blue colours (~ 10 per cent of the sample) which cannot be accounted for by the frosting scenario described above. Additionally, Rose CaII index results (Smith et al. in prep.) appear not to support the presence of young stellar populations ($\lesssim 1.5$ Gyr) in the majority of red sequence galaxies.

For most of this study, we have neglected the blue horizontal branch (BHB) as cluster red sequence galaxies have $[Z/H] \sim 0$. However, it is possible that a low metallicity population with a BHB morphology may be present in some galaxies (Maraston & Thomas 2000). Therefore, an alternative ‘frosting’ scenario consists of a low mass fraction, old, low metallicity, BHB stellar population embedded in a $[Z/H]=0$ galaxy. Estimates from the M05 models show that ‘frosting’ by a 4–5 per cent mass fraction population with $[Z/H]=-1.35$ could give an $NUV-J$ colour ~ 1 mag bluer, while changing the $B-R$ by only ~ 0.03 mag. The effect of the low-metallicity frosting on the derived spectroscopic age is

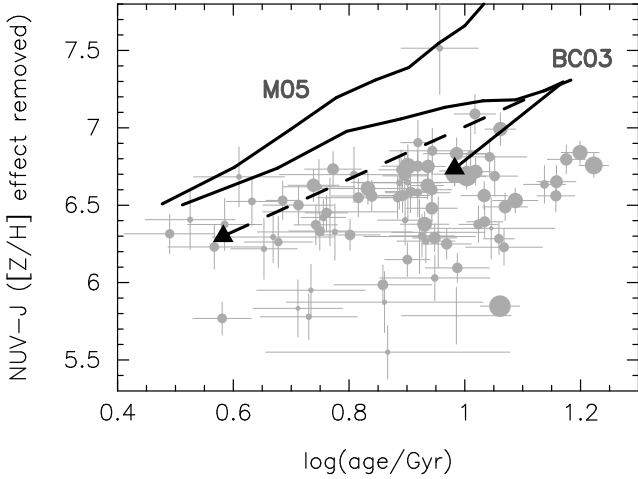


Figure 13. Simple stellar population tracks from the M05 and BC03 models shown in the context of the $NUV-J$ colour (correcting to $[Z/H]=0$ using the correlation from Fig. 6) vs $\log(\text{age})$. Vectors indicate two BC03 frosting scenarios with minor populations of $\{\mu, \text{age}\} = \{0.03, 1.5 \text{ Gyr}\}$ and $\{0.01, 0.7 \text{ Gyr}\}$ (solid and dashed vector respectively).

likely similar to the effect of frosting by a young component, since both cases are driven by increased A-star contribution to the Balmer lines.

4.4 NUV K-corrections

K-corrections for the UV bands are poorly constrained, as the spectral shape of galaxies at wavelengths shorter than $\sim 3000\text{\AA}$ is not well known. Previous studies of the UV CMR largely ignore the K-correction, or in the case of Yi et al. (2005, who estimate corrections of $0.1 - 0.2$ mag for $z = 0 - 0.25$) apply corrections based on the luminosity distance without considering the spectral shape of galaxies.

Kaviraj et al. (2006) compute NUV K-corrections for best fit model SEDs derived from SDSS and *GALEX* photometry. Corrections of ~ 0.1 mag were found for redshifts $z < 0.1$. However, corrections for their model of a 9 Gyr old simple stellar population are much larger ($0.4 - 1.0$ mag for $0.04 < z < 0.11$).

As an illustration, we calculate K-corrections from the models of Maraston (2005, M05) at various redshifts ($0.015 < z < 0.072$), both for simple populations and galaxies in the ‘frosting’ scenario described in Sec 4.3. K-corrections of $0.2 - 1.2$ mag are obtained, depending on the metallicity and age (increasing either increases the correction), and on the mass fraction of the young stellar component. The corrections are dominated by the 2640\AA spectral break (cf Eisenstein et al. 2003), which is redshifted completely out of the NUV band by $z \approx 0.07$. In Eisenstein et al., who study the average spectra of 726 luminous, red, SDSS galaxies at $0.47 < z < 0.55$, the break appears less prominent than in the M05 spectra (a ~ 50 per cent drop in flux as opposed to ~ 80 per cent).

Fig 14 shows the regression line residuals from the colour-magnitude diagram for the NFPS sample (Fig 2; upper panel) plotted against the galaxy redshift in the heliocentric frame. The solid line shows the expected trend if the M05 K-corrections were necessary, but not applied.

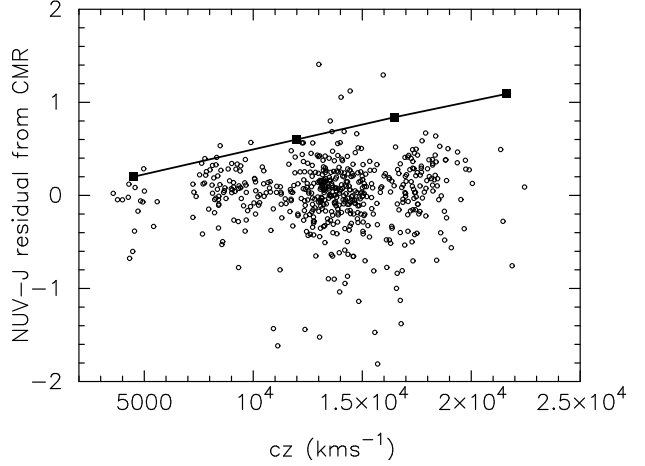


Figure 14. CMR residuals for the NFPS sample (Fig 2; upper panel) vs heliocentric galaxy redshift. The filled squares and solid line show the predicted trend if the K-corrections from the M05 models were necessary, but not applied.

This implies the uncorrected residuals should have a steep correlation with redshift, which is not observed. A flatter K-correction is preferred by the data, as in Kaviraj et al. (2006). Along with the Eisenstein et al. spectrum described above, this result highlights the uncertainty in the UV K-corrections (as well as the problems of stellar population models in the UV).

5 CONCLUSIONS

Using *GALEX* UV and 2MASS J band photometry, we have investigated the relationship between UV-IR colours and spectroscopically derived stellar population parameters (age, metallicity and α -abundance) for red sequence galaxies in local clusters.

We select galaxies using strict emission criteria to avoid contamination from galaxies with very recent star formation. We analyse the NUV colour-magnitude relation (CMR) for our two samples of quiescent galaxies (920 in NFPS; 156 in SSC), and find rms dispersions of 0.37 and 0.30 mag (intrinsic scatter of 0.36 and 0.29 mag) respectively. This is similar to previously reported values of ~ 0.5 mag and is an order of magnitude larger than the scatter in the optical CMR (~ 0.05 mag).

We compared the $NUV-J$ colour to the spectroscopic stellar population parameters for 87 galaxies in the SSC sample and found the following:

- There is a significant $NUV-J$ vs metallicity trend, with a slope of 1.27 ± 0.23 and an rms dispersion of 0.32 mag.
- There is only a weak $NUV-J$ vs age trend after the metallicity effect has been removed, and no correlation with α -abundance.
- There is a large intrinsic scatter (~ 0.25 mag) in the $NUV-J$ colour at fixed age and metallicity which cannot be easily accounted for with simple stellar populations.

The unexpected blue colours of at least some objects, including an influential outlier, cannot be attributed to large radius contamination from other objects, and aperture bias

cannot account for the large scatter. Corrections for the UV upturn (UVX) phenomenon are relatively small (~ 0.2 mag) and are similar galaxy-to-galaxy, so do not reduce the intrinsic scatter.

We find that the large *NUV-J* intrinsic scatter could be attributed to galaxy ‘frosting’ by small (< 5 per cent) populations of either young stars or a low metallicity blue horizontal branch.

ACKNOWLEDGMENTS

TDR is supported by the STFC Studentship PPA/S/S/2006/04341. RJS is supported by the rolling grant PP/C501568/1 ‘Extragalactic Astronomy and Cosmology at Durham 2005–2010’. Based on observations made with the NASA Galaxy Evolution Explorer. *GALEX* is operated for NASA by California Institute of Technology under NASA contract NAS-98034. This publication makes use of data products from the Two Micron All Sky Survey, which is a joint project of the University of Massachusetts and the Infrared Processing and Analysis Center/California Institute of Technology, funded by NASA and the National Science Foundation. We thank Chris Haines and the SOS team for providing the *B-R* colours used in Figures 5 and 9.

REFERENCES

- Bernardi M., Sheth R.K., Nichol R.C., Schneider D.P., Brinkmann J., 2005, *ApJ*, 129, 61
- Bertin E., Arnouts S., 1996, *A&A*, 117, 393B
- Blanton M. R. et al. 2005, *AJ*, 129, 2562
- Boselli A. et al., 2005, *ApJ*, 629, L29
- Bower R.G., Lucey J.R., Ellis R.S., 1992, *MNRAS*, 254, 601
- Bruzual G., Charlot S., 2003, *MNRAS*, 344, 1000
- Burstein D., Bertola F., Buson L., Faber S. M., Lauer T. R., 1988, *ApJ*, 328, 440
- Caldwell N., Rose J.A., Concannon K.D., 2003, *AJ*, 125, 289
- Cardelli J.A., Clayton G.C., Mathis J.S., 1989, *ApJ*, 345, 245
- Code A. D., 1969, *PASP*, 81, 482
- Donas J. et al., 2006, *arXiv:astro-ph/0608594*
- Dorman B., 1997, *ASPC*, 116, 195
- Dorman B., O’Connell R. W., Rood R. T., 2003, *ApJ*, 591, 878
- Dotter A., Chaboyer B., Ferguson J.W., Lee H.-C., Worthey G., Jevremovic D., Baron E., 2007, *ApJ*, 666, 403
- Dressler A., 1984, *ApJ*, 281, 512
- Eisenstein D. J. et al., 2003, *ApJ*, 585, 694
- Ferreras I., Silk J., 2000, *ApJ*, 541L, 37
- Haines C. P., Gargiulo A., Merluzzi P., 2007, *arXiv:0707.2361*
- Jarrett T. H., Chester T., Cutri R., Schneider S., Skrutskie M., Huchra J. P., 2000, *AJ*, 119, 2498
- Kaviraj S. et al., 2006, *arXiv:astro-ph/0601029*
- Kaviraj S., Rey S.-C., Rich R. M., Yoon S.-J., Yi S. K., 2007, *MNRAS*, 381, 74
- Kodama T., Arimoto N., 1997, *A&A*, 320, 41
- Kuntschner H., Davies R. L., 1998, *MNRAS*, 295L, 29
- Larson R. B., 1974, *MNRAS*, 169, 229
- Lee H.-C., Lee Y.-W., Gibson B.K., 2002, *ApJ*, 124, 2664
- Leitherer C. et al., 1999, *ApJS*, 123, 3
- Maraston C., Thomas D., 2000, *ApJ*, 541, 126
- Maraston C., 2005, *MNRAS*, 362, 799
- Martin D. C., et al. 2005, *ApJ*, 619, L1
- Mathews W. G., Baker J. C., 1971, *ApJ*, 170, 241
- Mercurio A. et al., 2006, *MNRAS*, 368, 109
- Morrissey P. et al., 2007, *arXiv:0706.0755*
- Nelan J. E., Smith R. J., Hudson M. J., Wegner G. A., Lucey J. R., Moore S. A. W., Quinney S. J., Suntzeff N. B., 2005, *ApJ*, 623, 137
- O’Connell R. W., 1999, *ARA&A*, 37, 603
- O’Connell R. W. et al., 1992, *ApJ*, 395L, 45
- Rampazzo R. et al., 2007, *arXiv:0707.2896*
- Rich R. M. et al., 2005, *ApJ*, 619, 107
- Salasnich B., Girardi L., Weiss A., Chiosi C., 2000, *A&A*, 361, 1023
- Salim S., et al., 2007, *arXiv:0704.3611*
- Sánchez-Blázquez P., Forbes D. A., Strader J., Brodie J., Proctor R., 2007, *MNRAS*, 377, 759
- Schawinski K. et al., 2006, *Nature*, 442, 888
- Schlegel D. J., Finkbeiner D. P., Davies M., 1998, *ApJ*, 500, 525
- Serra P., Trager S.C., 2007, *MNRAS*, 374, 769S
- Skrutskie M. F. et al., 2006, *ApJ*, 131, 1163
- Smith R. J. et al., 2004, *ApJ*, 128, 1558
- Smith R. J., Lucey J.R., Hudson M. J., 2007, *MNRAS*, 381, 1035
- Smith R. J., Lucey J.R., Hudson M. J., in prep.
- Tamura N., Ohta K., 2004, *MNRAS*, 355, 617
- Thomas D., Maraston C., Bender R., 2003, *MNRAS*, 339, 897
- Thomas D., Maraston C., Korn A., 2004, *MNRAS*, 351, L19
- Thomas D., Maraston C., Bender R., Mendes de Oliveira C., 2005, *ApJ*, 621, 673
- Trager S. C., Faber S. M., Worthey G., Gonzalez J. J., 2000, *AJ*, 120, 165
- Visvanathan N., Sandage A., 1977, *ApJ*, 216, 214
- Worthey G., 1994, *ApJS*, 95, 107
- Yi S., Demarque P., Oemler Jr A., 1997, *ApJ*, 486, 201
- Yi S. K. et al., 2005, *ApJ*, 619, L111